

Micromachined 95 GHz waveguide-fed plastic horn antennas

Firas Sammoura, Yiin-Kuen Fuh and Liwei Lin

Department of Mechanical Engineering, University of California, Berkeley, CA 94720, USA

Received 4 December 2007, in final form 19 February 2008

Published 1 April 2008

Online at stacks.iop.org/JMM/18/055009

Abstract

Waveguide-fed plastic horn antennas have been demonstrated for W-band applications using a versatile and cost-effective micro hot embossing process. The three-dimensional (3D) polymer structure with internally coated conductor is composed of a pyramidal horn, an E-plane waveguide bend, two resonant cavities for impedance matching and a connecting rectangular waveguide. Measurement results show broadband characteristics in W-band with a return loss of better than -10 dB; the bandwidth is 25.2 GHz between 76.5 and 101.7 GHz (26.5%), and the 3 dB beam widths of the E- and H-plane gain patterns at 95 GHz are 26° and 23° , respectively. The antenna gain is 17.04 dB at 95 GHz and the cross-polarization discriminations for E- and H-plane are 19.5 dB and 22.2 dB, respectively.

(Some figures in this article are in colour only in the electronic version)

1. Introduction

Conventional horn antennas and waveguides are made of three-dimensional (3D) metallic materials and generally have better power-carrying capabilities as compared with micro-strip-based coplanar architectures [1]. However, the mechanical manufacturing processes in making these 3D components are not cost-effective and the serial assembly process in making the whole system is time-consuming and labor intensive. Recently, micromachining technologies have been proposed to construct three-dimensional wireless components and systems massively and in parallel. For example, silicon micromachined antennas have been demonstrated by using anisotropic silicon etching to construct 3D horn flare angles by combining two wafers having V-shape grooves [2], by using silicon nitride membranes on top of open pyramidal cavities made by silicon wet etching process [3], or by using several layers of micromachined silicon to construct an octagonal horn antenna [4]. The flare angles of these antennas are limited by the crystalline orientation of silicon due to the anisotropic silicon etching processes. The LIGA process¹, on the other hand, has also been used to make a tapered slot antenna [5]. However, it is well known that the LIGA process is not suitable to make true 3D structures. A layer-by-layer electrochemical fabrication (EFAB) process has been used to build a miniature rectangular

¹ LIGA — Lithographie, Gavanoformung, Abformung in German for Lithography, Electroplating and Molding in English. A process developed in Germany to fabricate high-aspect-ratio microstructures.

coaxial transmission line for Ka band applications but a total of 41 layer processes is required [6]. Electroforming, on the other hand, has been used to demonstrate a single corrugated horn antenna in W-band [7]. However, the striping step from mandrel prohibits its application to make 3D-integrated structures such as combination of the horn antenna and waveguide network. Furthermore, the electroforming process results in heavier products as compared with polymer-based structures [8]. This paper proposes and demonstrates a simple, self-aligned plastic micro hot embossing technique with an internally coated metallic layer to construct millimeter-wave components. Topas[®]COC polymer was used as a polymeric material and electroplated gold was used as the conductor. A horn antenna fed by a 90° E-plane bend and connecting rectangular waveguide has been chosen as the demonstration example. Broadband attributes are demonstrated with the measured return loss of better than -10 dB from 76.5 GHz to 101.7 GHz.

2. Design parameters and the fabrication process

2.1. Design parameters and analysis

Figure 1 shows the schematic diagram of the proposed waveguide-fed horn antenna operating at 95 GHz. The design parameters are calculated according to conventional antenna theories [9], such as the height of the pyramidal horn (L_3); the length (a) and width (b) of the horn at its base in the E- and

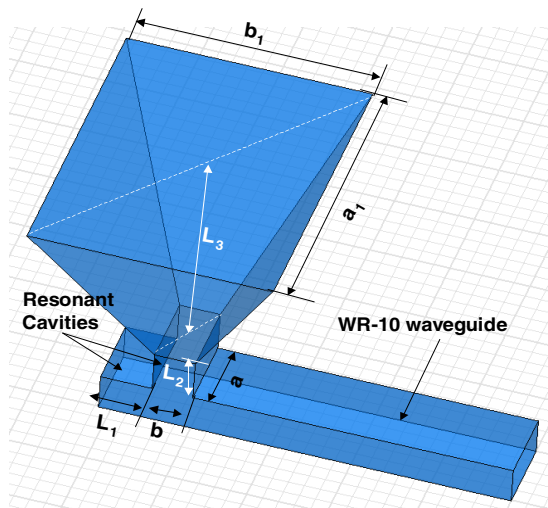


Figure 1. Proposed horn antenna fed by a 90° E-plane waveguide bend and a WR-10 rectangular waveguide.

H-plane, and the flared length (a_1) and width (b_1) of the horn at its distal end. A gain of 17 dB has been chosen as the proof-of-concept demonstration and a_1 , b_1 and L_3 are calculated as 10.11 mm, 7.69 mm and 7.13 mm, respectively [10]. The resonant cavities lengths L_1 and L_2 are designed to reduce the return loss due to the 90° E-plane bend between the connecting waveguide and the horn antenna. In the design process, some traditional matching approaches such as inductive posts have been considered [11]. Considering the simplicity in manufacturability/compatibility with the proposed plastic hot embossing process with traditional mechanical machining to make the mold inserts, resonant cavities are chosen with matching impedance with the horn antenna, E-plane bend and feeding waveguide.

Ansoft HFSS (high frequency structure simulator) was employed to simulate the return loss in the parametric study using the methodology of the direct search method, where L_1 is fixed first while L_2 is swept to get the optimal L_2 value for the best return loss performance. The simulation results of the return loss versus L_1 are plotted in figure 2(a), and the best impedance match of -9.7 dB is achieved when L_1 is equal to 1.61 mm. It is noted that the return loss versus L_1 is periodical with a period of about 2 mm, which corresponds to the half waveguide length at 95 GHz. Similar periodicity in resonant cavity L_2 is also observed in figure 2(b). Moreover, the matching capability of L_1 is more sensitive than L_2 as the peak-to-peak amplitudes are 9.23 dB and 6.01 dB per half guide wavelength for L_1 and L_2 , respectively. The process continues until a converging solution is achieved for both L_1 and L_2 . Using HFSS parametric simulations, the resonant lengths L_1 and L_2 are found as 1.61 mm and 1.41 mm, respectively, and the return loss, s_{11} , is simulated as -14.5 dB at 95 GHz. The field distribution can be very complex as a result of the horn antenna, resonant cavities and E-plane bend. Ansoft HFSS was used to further analyze the field distribution, including the magnitude and vector representation in the electric field as shown in figures 2(c)–(d). It is observed that the TE₁₀ mode

can be excited and transmitted through the E-plane waveguide bend at which the impedance is matched by adopting two resonant cavities and the horn antenna transmits a spherical wave with a field phase difference in the aperture.

2.2. Fabrication process

Figure 3 illustrates the self-aligned 3D plastic fabrication process. An upper mold insert is used to construct the horn patterns and a lower mold insert is used to construct the WR-10 rectangular waveguide (figure 3(a)). A self-aligned molding process is designed to have the alignment key on the upper mold insert and key slot on the lower mold insert for automatic self-alignment during the process. Both upper and lower mold inserts are made of aluminum using precision mechanical machines while the horn shape is made of steel and screwed to the upper mold insert. The self-aligned key and key slot have a tolerance of $12.5 \mu\text{m}$ such that the maximum possible misalignment is $25 \mu\text{m}$. The mold is heated to 160°C to be above the glass transition point of the Topas[®]COC 8007 polymer and a pressure of 156 MPa is applied [12]. At the end of the molding process, a thin layer of polymer residue of about $30 \mu\text{m}$ in thickness is found between the top and bottom mold inserts at the pyramidal horn and the waveguide intersection region although both mold inserts are ‘contacted’ in the molding process. This thin layer is removed using a razor blade and the process shown in figure 3(b) applies after these steps. This process typically results in polymer residues of $10 \mu\text{m}$ in terms of roughness around the perimeter of the hole. One alternative process is to use oxygen plasma to etch/clean and remove this residual layer but this process will cause the overall dimensional changes which could be compensated in the mold design. Afterward, a $200 \text{ \AA}/6000 \text{ \AA}$ of Cr/Pt is sputtered on both sides of substrates as the seed layer for the electroplating process (figure 3(c)). The continuity between the front and back sputtered layers is achieved by non-directional sputtering (rotating table in the sputtering system) and checked by resistivity measurement afterward. An aluminum substrate with a seed layer made of $200 \text{ \AA}/6000 \text{ \AA}$ of Cr/Pt is added at the bottom. A plastic flange adaptor is designed to connect the waveguide to the spectrum analyzer. It is separately fabricated using the same hot embossing process and is fitted at the waveguide end [13]. Super glue (Loctite quicktite) is used to fix the flange adaptor with the waveguide-fed antenna. The external surface of the flange facing the spectrum analyzer is planarized afterward using a lapping process with silicon carbide paper of very fine, 600-grid mesh. Finally, a selective electroplating and sealing process [14] is conducted to deposit an $8 \mu\text{m}$ thick gold layer on the internal surface of the antenna and to seal the system as shown in figure 3(d). Figure 3(e) shows an optical photo of a fabricated waveguide-fed horn antenna with a close-up view at the horn. During the sputtering and deposition process, Kapton tapes are applied manually as the masking material to cover areas that do not need the metallic coverage. As a result, about 1 mm wide electroplated gold layer is deposited around the horn edge on the top surface of the horn antenna as shown. Figure 3(f) shows the close-up view at the flange

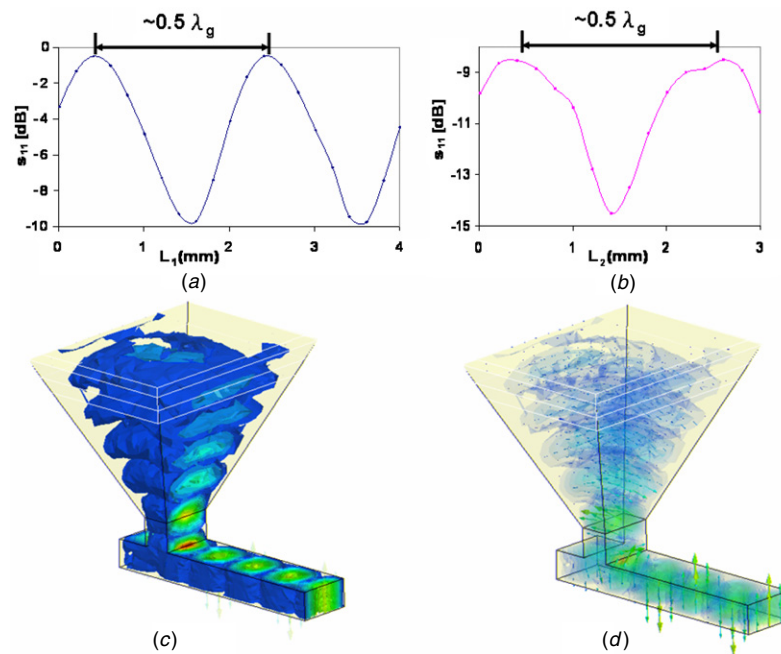


Figure 2. Parametric design using HFSS to calculate the s_{11} responses with respect to (a) the length of the first resonant cavity, L_1 , and (b) the length of the second resonant cavity, L_2 . (c) Magnitude and (d) vector plots of electric fields for TE_{10} polarization.

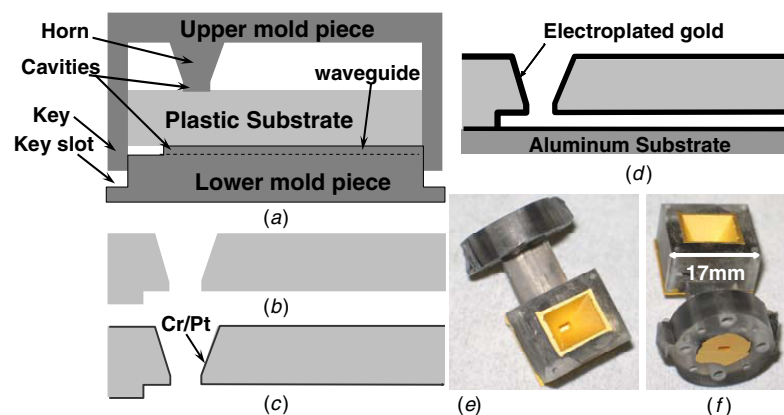


Figure 3. Fabrication process of the waveguide-fed horn antenna (a)–(d). Optical photos of the fabricated waveguide-fed horn antenna: close-up view at the (e) horn and (f) flange regions.

adaptor portion. The irregular electroplated gold layer on the surface of the flange is the result of the manual masking process using combinations of Kapton tapes.

3. Measurement results

As the manufacturing process inevitably introduced fabrication variations, the dimensions of the fabricated prototype are measured and compared with design values as shown in table 1. The main cause of variations is attributed to machining errors between the design and actual mold inserts and the differences in coefficient thermal expansion between polymer substrate ($0.7 \times 10^{-5} \text{ K}^{-1}$) and aluminum mold insert ($2.52 \times 10^{-5} \text{ K}^{-1}$). It is found that the biggest differences occur in the horn region, especially the flare width (a_1),

length (b_1) and horn height (L_3) as their final dimensions are -19% , -14% and 19% away from the design values in this prototype device. Figure 4 shows the simulation results of the E- and H-plane gain plot at 95 GHz using the design and fabricated dimensions. It is found that both co-polarized E- and H-plane radiation patterns from the design and fabricated geometries have minimum differences from the important central regions of -25° to $+25^\circ$. The design values result in directivity of 16.56 dB and the fabricated dimensions result in directivity of 17.02 dB. The reason for the minor increase in directivity from fabricated dimensions comes from the longer horn height, L_3 , which is the dominant factor in terms of antenna directivity. These simulation results demonstrate the robustness of the design to tolerate possible fabrication errors

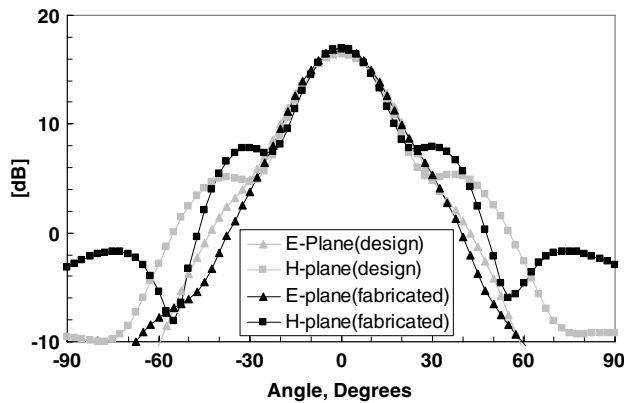


Figure 4. Simulation results of antenna radiation patterns at 95 GHz for E- and H-planes based on design and fabricated dimensions, respectively.

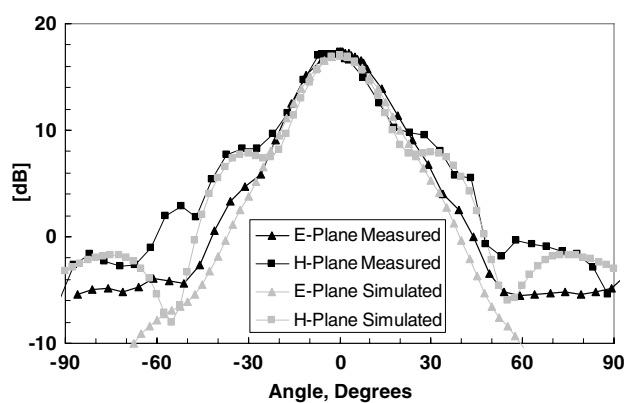


Figure 5. Simulation and measured radiation patterns of the antenna for the co-polarized (a) E- and (b) H-planes.

Table 1. Antenna parameter dimensions (in mm).

Parameter	Design	Mold insert	Complete device
A	2.54	2.48 ± 0.02	2.46 ± 0.02
B	1.27	1.27 ± 0.02	1.26 ± 0.02
A ₁	10.11	9.93 ± 0.03	9.92 ± 0.03
B ₁	7.69	7.56 ± 0.03	7.55 ± 0.03
L ₁	1.61	1.53 ± 0.02	1.52 ± 0.02
L ₂	1.41	1.33 ± 0.02	1.32 ± 0.02
L ₃	7.13	7.1 ± 0.03	7.32 ± 0.03

from micromachining processes, including the shrinkage of the polymer materials.

The radiation patterns of the horn antenna are measured using a millimeter-wave source (Micro-Now Instrument Company Inc., Model 705B Millimeter-wave sweeper/power supply) and a power meter (Millitech Inc., power meter type DPM-01, sensor type PMH-10M). For wave propagating at 95 GHz, the desirable distance in the far-field region is at least 12 cm and the distance between the two antennas was set as 19 cm. Figure 5 shows the simulated (based on the fabricated dimensions) and measured radiation patterns of the antenna between -90° and $+90^\circ$ for both co-polarized E- and H-plane, respectively. The radiation patterns in both planes agree relatively well between simulation and measurement

results between -50° and $+50^\circ$, indicating the effectiveness of design methodology and fabrication process. The measured 3 dB beam widths of the E- and H-plane patterns are 26° and 23° , respectively. For antennas with one narrow major lobe and one negligible minor lobe, the antenna directivity can be approximated using the half-power beam widths in radians measured in two perpendicular planes [9]. At 95 GHz, the directivity based on the measured 3 dB beam width is calculated at 17.33 dB as compared with simulation results at 17.02 dB. The calculated directivity based on the 3 dB beam width is larger than the simulated directivity and several factors may contribute to this discrepancy. First, directivity approximation uses the half-power method and experimental and/or simulation errors can affect the beam-width values. Second, the alignment accuracy between the reference antenna and the antenna to be characterized can also affect the experimental result. Nevertheless, the measurement results verify the design principles on the E-plane bend pyramidal antenna with connecting rectangular waveguide and that the polymeric antenna can be functional similar to a metallic antenna.

The ratio of the total received power relative to the total transmitted power of the receiver and transmitter antennas separated by a distance can be calculated by using the gains of the transmitting and receiving antennas [9]. It is found that the total transmitted power of the reference antenna is at 17.7 dBm with a standard gain of 20 dB and the efficiency of the prototype plastic waveguide-fed antenna is calculated as 86% as compared with the state-of-the-art metallic antennas at around 95%. Therefore the antenna gain is calculated from the product of directivity and antenna efficiency and the calculated gain is 17.04 dB, which agrees well with Ansoft HFSS simulation result of 17.42 dB. The gain obtained from measurement is slightly lower than the simulated value and the reason is mainly attributed to the additional losses that are associated with the surface roughness of the metallic electroplating as well as mismatch at the interface of the flange adaptor. We believe the gain and efficiency of the prototype plastic antenna can be further improved by addressing issues such as roughness of electroplated metallic layer, signal leakages to possible gaps created in the electroplating and sealing process and energy losses at the interface of the flange adaptor.

The co-polarized and cross-polarized radiation fields in the H- and E-planes are measured and compared as shown in figure 6. The cross-polarized H-plane radiation pattern is lower by about 22.2 dB than the corresponding co-polarized field at the maximum radiation point and is recorded between -30° and $+30^\circ$. Outside this range, the received power dropped below the measurement limit of the power meter. Similar characteristics are also observed in the E-plane radiation pattern in which the cross-polarized field is lower by about 19.5 dB than the corresponding co-polarized field at the maximum radiation point and is recorded between the -10° and $+10^\circ$ range. The cross-polarization discrimination is observed for both planes with better than 19.5 dB discrimination at broadside. The result verifies that the horn antenna is robust in rejecting radiations with different polarizations.

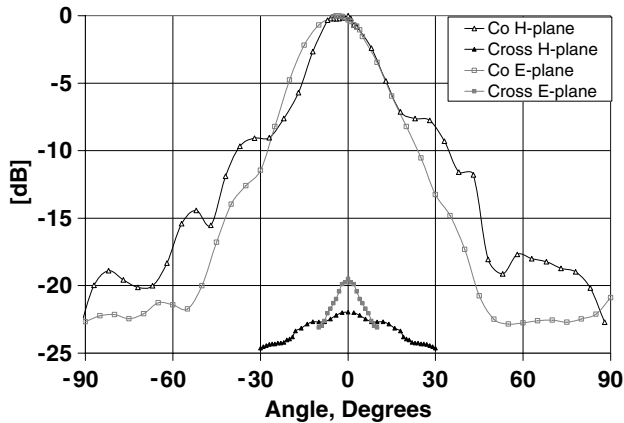


Figure 6. Measured radiation patterns of the horn antenna from the E- and H-plane co-polarized and cross-polarized fields.

The return loss, s_{11} , of the waveguide-fed horn antenna is measured using an Anritsu ME7808B network analyzer and compared with simulation result using HFSS as shown in figure 7. The return loss, s_{11} , at 95 GHz is measured to be -17.5 dB and the measured return loss of better than -10 dB demonstrates broadband attributes with a bandwidth of 25.2 GHz (26.5%) between 76.5 and 101.7 GHz. It is noted that the measured return loss is better than the simulated return loss by about 3 dB. One possible reason is the extra 1 mm wide gold layer deposited on top of the horn antenna as shown in figure 2(e) is not accounted for in the simulation and it may help the transition from the horn antenna to the outer space to increase the transmission and reduce the return loss. A second simulation is conducted to include the effect of the extra 1 mm wide gold layer. From the simulation results, an average of 2 dB lower return loss is observed as compared to the model without the extra gold layer as shown in figure 7.

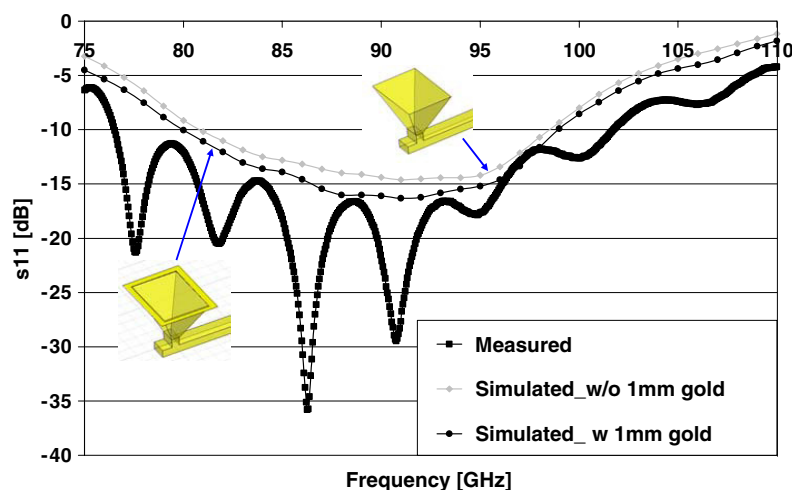


Figure 7. Simulated and measured return loss of the waveguide-fed horn antenna.

4. Conclusion

Waveguide-fed, plastic horn antennas have been demonstrated for W-band operation using a self-aligned 3D plastic hot embossing process. Several conclusions can be drawn from this work. First, a polymeric horn antenna fabricated by the proposed self-aligned embossing process has been demonstrated and the measurement results matched well with design and simulation patterns. Second, the fabrication process of the prototype device is not well controlled and results in three of the fabricated dimensions to be more than 10% off the design values. However, the simulated and measured radiation patterns do not deviate much from that of the designed dimensions within the $\pm 25^\circ$ regions. Third, E-plane bend, direct waveguide connection to a horn antenna has been shown to be functional as an alternative way for the integration of the antenna and waveguide systems, which is potentially very useful for the integrated polymeric fabrication process as demonstrated in this work. Finally, broadband characteristics in the W-band can be achieved with the proposed polymeric, E-plane waveguide bend, horn antenna operating at 95 GHz. We believe the proposed self-aligned embossing process can be further developed toward a full antenna array with built-in microstructures such as micro iris structures for filters [15] and micro membrane structures for phase shifters [16].

Acknowledgments

The authors would like to thank Professors Jack Welch of UC Berkeley and JC Chiao of University of Texas, Arlington for valuable discussions and Mr Kent Potter of the California Institute of Technology for the experimental measurements. This project is supported in part by an NSF grant DMI-0428884 and these devices were fabricated in the UC-Berkeley Microfabrication Laboratory and the Mechanical Engineering Machine Shop.

References

- [1] David M P 1997 *Microwave Engineering* (New York: Wiley)
- [2] Shenouda B A, Pearson L W and Harriss J E 2001 Etched-silicon micromachined-band waveguides and horn antennas *IEEE Trans. Microw. Theory Tech.* **49** 724–7
- [3] Rebeiz G M, Kasilingam D P, Guo Y, Stimson P A and Tutledge D B 1990 Monolithic millimeter-wave two-dimensional horn imaging array *IEEE Trans. Antennas Propag.* **38** 1473–82
- [4] Hesler J L *et al* 2001 Analysis of an octagonal micromachined horn antenna for submillimeter-wave applications *IEEE Trans. Antennas Propag.* **49** 997–1001
- [5] Gearhard S G and Willke T 1998 Integrated antennas and filters fabricated using micromachining techniques *IEEE Aerospace Applications Conf. Proc.* vol 3 pp 249–54
- [6] Brown E R, Cohen A L, Bang C A, Lockard M S, Byrne B W, Vandelli N M, McPherson D S and Zhang G 2004 Characteristics of microfabricated rectangular coax in the Ka band *Microw. Opt. Technol. Lett.* **40** 365–8
- [7] Benigual Y, Berthon A, Klooster C V and Costes L 2005 Design realization and measurements of a high performance wide-band corrugated horn *IEEE Trans. Antennas Propag.* **53** 3540–6
- [8] Kuo S, Roberts A, Ingram J and Eglitis I 2004 A Compact, Circularly Polarized Horn Antenna AIAA-2004–3265 (Redondo Beach, CA: Northrop Grumman Space Technology)
- [9] Balanis C A 1997 *Antenna Theory: Analysis and Design* (New York: Wiley) pp 651–721
- [10] Sammoura F 2006 Micromachined plastic millimeter-wave radar components *PhD Thesis* University of California, Berkeley
- [11] Mizutani A *et al* 2007 Grating lobe suppression of narrow-wall slotted hollow waveguide millimeter-wave planar antenna for arbitrary linear polarization *IEEE Trans. Antennas Propag.* **55** 313–20
- [12] Shen X-J, Pan L-W and Lin L 2002 Microplastic embossing process: experimental and theoretical characterizations *Sensors Actuators A* **97–8** 428–33
- [13] Sammoura F, Su Y-C, Cai Y, Chi C-Y, Elamran B, Lin L and Chiao J-C 2006 Plastic 95 GHz rectangular waveguides by micro molding technologies *Sensors Actuators* **127** 270–5
- [14] Pan L W and Lin L 2001 Batch transfer of LIGA microstructures by selective electroplating and bonding *IEEE/ASME J. Microelectromech. Syst.* **10** 25–32
- [15] Sammoura F, Cai Y, Chi C-Y, Hirano T, Lin L and Chiao J-C 2005 A micromachined W-band iris filter *13th Int. Conf. Solid-State Sensors, Actuators and Microsystems (Seoul, Korea, 5–9 June)* pp 1067–70
- [16] Sammoura F and Lin L 2007 A plastic W-band MEMS phase shifter *14th Int. Conf. Solid-State Sensors, Actuators and Microsystems (Lyon, France, 10–14 June)* pp 647–50